DESY-03-212
December 2003
Revised September 2006

Beauty photoproduction measured using decays into muons in dijet events in ep collisions at $\sqrt{s} = 318\,\mathbf{GeV}$

ZEUS Collaboration

Abstract

The photoproduction of beauty quarks in events with two jets and a muon has been measured with the ZEUS detector at HERA using an integrated luminosity of 110 pb^{-1}. The fraction of jets containing b quarks was extracted from the transverse momentum distribution of the muon relative to the closest jet. Differential cross sections for beauty production as a function of the transverse momentum and pseudorapidity of the muon, of the associated jet and of x_γ^{jets}, the fraction of the photon's momentum participating in the hard process, are compared with MC models and QCD predictions made at next-to-leading order. The latter give a good description of the data.

The ZEUS Collaboration

S. Chekanov, M. Derrick, D. Krakauer, J.H. Loizides[1], S. Magill, S. Miglioranzi[1], B. Musgrave, J. Repond, R. Yoshida
Argonne National Laboratory, Argonne, Illinois 60439-4815, USA [n]

M.C.K. Mattingly
Andrews University, Berrien Springs, Michigan 49104-0380, USA

P. Antonioli, G. Bari, M. Basile, L. Bellagamba, D. Boscherini, A. Bruni, G. Bruni, G. Cara Romeo, L. Cifarelli, F. Cindolo, A. Contin, M. Corradi, S. De Pasquale, P. Giusti, G. Iacobucci, A. Margotti, A. Montanari, R. Nania, F. Palmonari, A. Pesci, G. Sartorelli, A. Zichichi
University and INFN Bologna, Bologna, Italy [e]

G. Aghuzumtsyan, D. Bartsch, I. Brock, S. Goers, H. Hartmann, E. Hilger, P. Irrgang, H.-P. Jakob, O. Kind, U. Meyer, E. Paul[2], J. Rautenberg, R. Renner, A. Stifutkin, J. Tandler, K.C. Voss, M. Wang, A. Weber[3]
Physikalisches Institut der Universität Bonn, Bonn, Germany [b]

D.S. Bailey[4], N.H. Brook, J.E. Cole, G.P. Heath, T. Namsoo, S. Robins, M. Wing
H.H. Wills Physics Laboratory, University of Bristol, Bristol, United Kingdom [m]

M. Capua, A. Mastroberardino, M. Schioppa, G. Susinno
Calabria University, Physics Department and INFN, Cosenza, Italy [e]

J.Y. Kim, Y.K. Kim, J.H. Lee, I.T. Lim, M.Y. Pac[5]
Chonnam National University, Kwangju, Korea [g]

A. Caldwell[6], M. Helbich, X. Liu, B. Mellado, Y. Ning, S. Paganis, Z. Ren, W.B. Schmidke, F. Sciulli
Nevis Laboratories, Columbia University, Irvington on Hudson, New York 10027 [o]

J. Chwastowski, A. Eskreys, J. Figiel, A. Galas, K. Olkiewicz, P. Stopa, L. Zawiejski
Institute of Nuclear Physics, Cracow, Poland [i]

L. Adamczyk, T. Bołd, I. Grabowska-Bołd[7], D. Kisielewska, A.M. Kowal, M. Kowal, T. Kowalski, M. Przybycień, L. Suszycki, D. Szuba, J. Szuba[8]
Faculty of Physics and Nuclear Techniques, AGH-University of Science and Technology, Cracow, Poland [p]

A. Kotański[9], W. Słomiński
Department of Physics, Jagellonian University, Cracow, Poland

V. Adler, U. Behrens, I. Bloch, K. Borras, V. Chiochia, D. Dannheim, G. Drews, J. Fourletova, U. Fricke, A. Geiser, P. Göttlicher[10], O. Gutsche, T. Haas, W. Hain, S. Hillert[11], B. Kahle, U. Kötz, H. Kowalski[12], G. Kramberger, H. Labes, D. Lelas, H. Lim, B. Löhr, R. Mankel, I.-A. Melzer-Pellmann, C.N. Nguyen, D. Notz, A.E. Nuncio-Quiroz, A. Polini, A. Raval, L. Rurua, U. Schneekloth, U. Stösslein, G. Wolf, C. Youngman, W. Zeuner
Deutsches Elektronen-Synchrotron DESY, Hamburg, Germany

S. Schlenstedt
DESY Zeuthen, Zeuthen, Germany

G. Barbagli, E. Gallo, C. Genta, P. G. Pelfer
University and INFN, Florence, Italy [e]

A. Bamberger, A. Benen, F. Karstens, D. Dobur, N.N. Vlasov
Fakultät für Physik der Universität Freiburg i.Br., Freiburg i.Br., Germany [b]

M. Bell, P.J. Bussey, A.T. Doyle, J. Ferrando, J. Hamilton, S. Hanlon, D.H. Saxon, I.O. Skillicorn
Department of Physics and Astronomy, University of Glasgow, Glasgow, United Kingdom [m]

I. Gialas
Department of Engineering in Management and Finance, Univ. of Aegean, Greece

T. Carli, T. Gosau, U. Holm, N. Krumnack, E. Lohrmann, M. Milite, H. Salehi, P. Schleper, S. Stonjek[11], K. Wichmann, K. Wick, A. Ziegler, Ar. Ziegler
Hamburg University, Institute of Exp. Physics, Hamburg, Germany [b]

C. Collins-Tooth, C. Foudas, R. Gonçalo[13], K.R. Long, A.D. Tapper
Imperial College London, High Energy Nuclear Physics Group, London, United Kingdom [m]

P. Cloth, D. Filges
Forschungszentrum Jülich, Institut für Kernphysik, Jülich, Germany

M. Kataoka[14], K. Nagano, K. Tokushuku[15], S. Yamada, Y. Yamazaki
Institute of Particle and Nuclear Studies, KEK, Tsukuba, Japan [f]

A.N. Barakbaev, E.G. Boos, N.S. Pokrovskiy, B.O. Zhautykov
Institute of Physics and Technology of Ministry of Education and Science of Kazakhstan, Almaty, Kazakhstan

D. Son
Kyungpook National University, Center for High Energy Physics, Daegu, South Korea [g]

K. Piotrzkowski
Institut de Physique Nucléaire, Université Catholique de Louvain, Louvain-la-Neuve, Belgium

F. Barreiro, C. Glasman[16], O. González, L. Labarga, J. del Peso, E. Tassi, J. Terrón, M. Vázquez, M. Zambrana
Departamento de Física Teórica, Universidad Autónoma de Madrid, Madrid, Spain [l]

M. Barbi, F. Corriveau, S. Gliga, J. Lainesse, S. Padhi, D.G. Stairs, R. Walsh
Department of Physics, McGill University, Montréal, Québec, Canada H3A 2T8 [a]

T. Tsurugai
Meiji Gakuin University, Faculty of General Education, Yokohama, Japan [f]

A. Antonov, P. Danilov, B.A. Dolgoshein, D. Gladkov, V. Sosnovtsev, S. Suchkov
Moscow Engineering Physics Institute, Moscow, Russia [j]

R.K. Dementiev, P.F. Ermolov, Yu.A. Golubkov[17], I.I. Katkov, L.A. Khein, I.A. Korzhavina, V.A. Kuzmin, B.B. Levchenko[18], O.Yu. Lukina, A.S. Proskuryakov, L.M. Shcheglova, S.A. Zotkin
Moscow State University, Institute of Nuclear Physics, Moscow, Russia [k]

N. Coppola, S. Grijpink, E. Koffeman, P. Kooijman, E. Maddox, A. Pellegrino, S. Schagen, H. Tiecke, J.J. Velthuis, L. Wiggers, E. de Wolf
NIKHEF and University of Amsterdam, Amsterdam, Netherlands [h]

N. Brümmer, B. Bylsma, L.S. Durkin, T.Y. Ling
Physics Department, Ohio State University, Columbus, Ohio 43210 [n]

A.M. Cooper-Sarkar, A. Cottrell, R.C.E. Devenish, B. Foster, G. Grzelak, C. Gwenlan[19], S. Patel, P.B. Straub, R. Walczak
Department of Physics, University of Oxford, Oxford United Kingdom [m]

A. Bertolin, R. Brugnera, R. Carlin, F. Dal Corso, S. Dusini, A. Garfagnini, S. Limentani, A. Longhin, A. Parenti, M. Posocco, L. Stanco, M. Turcato
Dipartimento di Fisica dell' Università and INFN, Padova, Italy [e]

E.A. Heaphy, F. Metlica, B.Y. Oh, J.J. Whitmore[20]
Department of Physics, Pennsylvania State University, University Park, Pennsylvania 16802 [o]

Y. Iga
Polytechnic University, Sagamihara, Japan [f]

G. D'Agostini, G. Marini, A. Nigro
Dipartimento di Fisica, Università 'La Sapienza' and INFN, Rome, Italy [e]

C. Cormack[21], J.C. Hart, N.A. McCubbin
Rutherford Appleton Laboratory, Chilton, Didcot, Oxon, United Kingdom [m]

C. Heusch
University of California, Santa Cruz, California 95064, USA [n]

I.H. Park
Department of Physics, Ewha Womans University, Seoul, Korea

N. Pavel
Fachbereich Physik der Universität-Gesamthochschule Siegen, Germany

H. Abramowicz, A. Gabareen, S. Kananov, A. Kreisel, A. Levy
Raymond and Beverly Sackler Faculty of Exact Sciences, School of Physics, Tel-Aviv University, Tel-Aviv, Israel [d]

M. Kuze
Department of Physics, Tokyo Institute of Technology, Tokyo, Japan [f]

T. Fusayasu, S. Kagawa, T. Kohno, T. Tawara, T. Yamashita
Department of Physics, University of Tokyo, Tokyo, Japan [f]

R. Hamatsu, T. Hirose[2], M. Inuzuka, H. Kaji, S. Kitamura[22], K. Matsuzawa
Tokyo Metropolitan University, Department of Physics, Tokyo, Japan [f]

M.I. Ferrero, V. Monaco, R. Sacchi, A. Solano
Università di Torino and INFN, Torino, Italy [e]

M. Arneodo, M. Ruspa
Università del Piemonte Orientale, Novara, and INFN, Torino, Italy [e]

T. Koop, J.F. Martin, A. Mirea
Department of Physics, University of Toronto, Toronto, Ontario, Canada M5S 1A7 [a]

J.M. Butterworth[23], R. Hall-Wilton, T.W. Jones, M.S. Lightwood, M.R. Sutton[4], C. Targett-Adams
Physics and Astronomy Department, University College London, London, United Kingdom [m]

J. Ciborowski[24], R. Ciesielski[25], P. Łużniak[26], R.J. Nowak, J.M. Pawlak, J. Sztuk[27], T. Tymieniecka[28], A. Ukleja[28], J. Ukleja[29], A.F. Żarnecki
Warsaw University, Institute of Experimental Physics, Warsaw, Poland [q]

M. Adamus, P. Plucinski
Institute for Nuclear Studies, Warsaw, Poland [q]

Y. Eisenberg, L.K. Gladilin[30], D. Hochman, U. Karshon M. Riveline
Department of Particle Physics, Weizmann Institute, Rehovot, Israel [c]

D. Kçira, S. Lammers, L. Li, D.D. Reeder, M. Rosin, A.A. Savin, W.H. Smith
Department of Physics, University of Wisconsin, Madison, Wisconsin 53706, USA [n]

A. Deshpande, S. Dhawan
Department of Physics, Yale University, New Haven, Connecticut 06520-8121, USA [n]

S. Bhadra, C.D. Catterall, S. Fourletov, G. Hartner, S. Menary, M. Soares, J. Standage
Department of Physics, York University, Ontario, Canada M3J 1P3 [a]

[1] also affiliated with University College London, London, UK
[2] retired
[3] self-employed
[4] PPARC Advanced fellow
[5] now at Dongshin University, Naju, Korea
[6] now at Max-Planck-Institut für Physik, München,Germany
[7] partly supported by Polish Ministry of Scientific Research and Information Technology, grant no. 2P03B 122 25
[8] partly supp. by the Israel Sci. Found. and Min. of Sci., and Polish Min. of Scient. Res. and Inform. Techn., grant no.2P03B12625
[9] supported by the Polish State Committee for Scientific Research, grant no. 2 P03B 09322
[10] now at DESY group FEB
[11] now at Univ. of Oxford, Oxford/UK
[12] on leave of absence at Columbia Univ., Nevis Labs., N.Y., US A
[13] now at Royal Holoway University of London, London, UK
[14] also at Nara Women's University, Nara, Japan
[15] also at University of Tokyo, Tokyo, Japan
[16] Ramón y Cajal Fellow
[17] now at HERA-B
[18] partly supported by the Russian Foundation for Basic Research, grant 02-02-81023
[19] PPARC Postdoctoral Research Fellow
[20] on leave of absence at The National Science Foundation, Arlington, VA, USA
[21] now at Univ. of London, Queen Mary College, London, UK
[22] present address: Tokyo Metropolitan University of Health Sciences, Tokyo 116-8551, Japan
[23] also at University of Hamburg, Alexander von Humboldt Fellow
[24] also at Łódź University, Poland
[25] supported by the Polish State Committee for Scientific Research, grant no. 2 P03B 07222
[26] Łódź University, Poland
[27] Łódź University, Poland, supported by the KBN grant 2P03B12925
[28] supported by German Federal Ministry for Education and Research (BMBF), POL 01/043
[29] supported by the KBN grant 2P03B12725
[30] on leave from MSU, partly supported by University of Wisconsin via the U.S.-Israel BSF

[a] supported by the Natural Sciences and Engineering Research Council of Canada (NSERC)

[b] supported by the German Federal Ministry for Education and Research (BMBF), under contract numbers HZ1GUA 2, HZ1GUB 0, HZ1PDA 5, HZ1VFA 5

[c] supported by the MINERVA Gesellschaft für Forschung GmbH, the Israel Science Foundation, the U.S.-Israel Binational Science Foundation and the Benozyio Center for High Energy Physics

[d] supported by the German-Israeli Foundation and the Israel Science Foundation

[e] supported by the Italian National Institute for Nuclear Physics (INFN)

[f] supported by the Japanese Ministry of Education, Culture, Sports, Science and Technology (MEXT) and its grants for Scientific Research

[g] supported by the Korean Ministry of Education and Korea Science and Engineering Foundation

[h] supported by the Netherlands Foundation for Research on Matter (FOM)

[i] supported by the Polish State Committee for Scientific Research, grant no. 620/E-77/SPB/DESY/P-03/DZ 117/2003-2005

[j] partially supported by the German Federal Ministry for Education and Research (BMBF)

[k] partly supported by the Russian Ministry of Industry, Science and Technology through its grant for Scientific Research on High Energy Physics

[l] supported by the Spanish Ministry of Education and Science through funds provided by CICYT

[m] supported by the Particle Physics and Astronomy Research Council, UK

[n] supported by the US Department of Energy

[o] supported by the US National Science Foundation

[p] supported by the Polish State Committee for Scientific Research, grant no. 112/E-356/SPUB/DESY/P-03/DZ 116/2003-2005,2 P03B 13922

[q] supported by the Polish State Committee for Scientific Research, grant no. 115/E-343/SPUB-M/DESY/P-03/DZ 121/2001-2002, 2 P03B 07022

1 Introduction

The production of beauty quarks in ep collisions at HERA is a stringent test for perturbative Quantum Chromodynamics (QCD) since the large b-quark mass ($m_b \sim 5\,\text{GeV}$) provides a hard scale that should ensure reliable predictions. When Q^2, the negative squared four-momentum exchanged at the electron vertex, is small the reaction $ep \to e' b\bar{b} X$ can be considered as a photoproduction process in which a quasi-real photon, emitted by the incoming electron, interacts with the proton.

For b-quark transverse momenta comparable to the b-quark mass, next-to-leading-order (NLO) QCD calculations in which the b quark is generated dynamically are expected to provide accurate predictions for b photoproduction [1]. The corresponding leading-order (LO) QCD processes are the direct-photon process, in which the quasi-real photon enters directly in the hard interaction, $\gamma g \to b\bar{b}$, and the resolved-photon process, in which the photon acts as a source of partons that take part in the hard interaction ($gg \to b\bar{b}$ or $q\bar{q} \to b\bar{b}$).

The beauty-production cross section has been measured in $p\overset{(-)}{p}$ collisions at the ISR [2], S$p\bar{p}$S [3] and Tevatron colliders [4], in $\gamma\gamma$ interactions at LEP [5] and in fixed-target πN [6] and pN [7] experiments. Apart from the S$p\bar{p}$S data and the fixed-target experiments, the results were significantly above the NLO QCD prediction. The H1 measurement in ep interactions at HERA [8] found a cross section significantly larger than the prediction. The previous ZEUS measurement [9] was above, but consistent with, the prediction.

This paper reports a measurement of beauty photoproduction in events with two jets and a muon, $ep \to e'\, b\bar{b}\, X \to e'\, jj\mu\, X'$, for $Q^2 < 1\,\text{GeV}^2$.

2 Experimental set-up

The data sample used in this analysis corresponds to an integrated luminosity $\mathcal{L} = 110.4 \pm 2.2\ \text{pb}^{-1}$, collected by the ZEUS detector in the years 1996-1997 and 1999-2000. During the 1996-97 data taking, HERA provided collisions between an electron[1] beam of $E_e = 27.5\,\text{GeV}$ and a proton beam of $E_p = 820\,\text{GeV}$, corresponding to a centre-of-mass energy $\sqrt{s} = 300\,\text{GeV}$ ($\mathcal{L}_{300} = 38.0 \pm 0.6\ \text{pb}^{-1}$). In the years 1999-2000, the proton-beam energy was $E_p = 920\,\text{GeV}$, corresponding to $\sqrt{s} = 318\,\text{GeV}$ ($\mathcal{L}_{318} = 72.4 \pm 1.6\ \text{pb}^{-1}$).

A detailed description of the ZEUS detector can be found elsewhere [10]. A brief outline of the components that are most relevant for this analysis is given below.

[1] Electrons and positrons are not distinguished in this paper and are both referred to as electrons.

Charged particles are tracked in the central tracking detector (CTD) [11], which operates in a magnetic field of 1.43 T provided by a thin superconducting solenoid. The CTD consists of 72 cylindrical drift chamber layers, organized in nine superlayers covering the polar-angle[2] region $15^\circ < \theta < 164^\circ$. The transverse-momentum resolution for full-length tracks is $\sigma(p_T)/p_T = 0.0058p_T \oplus 0.0065 \oplus 0.0014/p_T$, with p_T in GeV.

The high-resolution uranium-scintillator calorimeter (CAL) [12] consists of three parts: the forward (FCAL), the barrel (BCAL) and the rear (RCAL) calorimeters. Each part is subdivided transversely into towers and longitudinally into one electromagnetic section (EMC) and either one (in RCAL) or two (in BCAL and FCAL) hadronic sections (HAC). The smallest subdivision of the calorimeter is called a cell. The CAL energy resolutions, as measured under test-beam conditions, are $\sigma(E)/E = 0.18/\sqrt{E}$ for electrons and $\sigma(E)/E = 0.35/\sqrt{E}$ for hadrons, with E in GeV.

The muon system consists of rear, barrel (R/BMUON) [13] and forward (FMUON) [10] tracking detectors. The B/RMUON consists of limited-streamer (LS) tube chambers placed behind the BCAL (RCAL), inside and outside a magnetized iron yoke surrounding the CAL. The barrel and rear muon chambers cover polar angles from 34° to 135° and from 135° to 171°, respectively. The FMUON consists of six trigger planes of LS tubes and four planes of drift chambers covering the angular region from 5° to 32°. The muon system exploits the magnetic field of the iron yoke and, in the forward direction, of two iron toroids magnetized to ~ 1.6 T to provide an independent measurement of the muon momentum.

The luminosity was measured using the bremsstrahlung process $ep \to ep\gamma$. The resulting small-angle energetic photons were measured by the luminosity monitor [14], a lead-scintillator calorimeter placed in the HERA tunnel at $Z = -107$ m.

3 Data Selection

The data were selected online by requiring either a high-momentum muon reaching the external B/RMUON chambers or two jets reconstructed in the CAL. A dedicated trigger requiring two jets and a muon with looser jet and muon thresholds was also used in the last part of the data taking.

Muons were reconstructed offline using the following procedure: a muon track was found in the inner and outer B/RMUON chambers or crossing at least 4 FMUON planes, then a

[2] The ZEUS coordinate system is a right-handed Cartesian system, with the Z axis pointing in the proton beam direction, referred to as the "forward direction", and the X axis pointing left towards the centre of HERA. The coordinate origin is at the nominal interaction point.

match in position and momentum to a CTD track was required. The angular acceptance of the F/B/RMUON and of the CTD, and the requirement that the muons reach the external chambers define three regions of good acceptance:

$$\begin{array}{rll} \text{rear} & -1.6 < \eta^\mu < -0.9, & p^\mu > 2.5\,\text{GeV}; \\ \text{barrel} & -0.9 < \eta^\mu < 1.3, & p_T^\mu > 2.5\,\text{GeV}; \\ \text{forward} & 1.48 < \eta^\mu < 2.3, & p^\mu > 4\,\text{GeV},\ p_T^\mu > 1\,\text{GeV}; \end{array} \quad (1)$$

where η^μ, p^μ and p_T^μ are the muon pseudorapidity, momentum and transverse momentum, respectively.

The hadronic system (including the muon) was reconstructed from energy-flow objects (EFOs) [15] which combine the information from calorimetry and tracking, corrected for energy loss in dead material. A reconstructed four-momentum $(p_X^i, p_Y^i, p_Z^i, E^i)$ was assigned to each EFO.

Jets were reconstructed from EFOs using the k_T algorithm [16] in the longitudinally invariant mode [17]. The E recombination scheme, which produces massive jets whose four-momenta are the sum of the four-momenta of the clustered objects, was used. Muons were associated with jets by the k_T algorithm: if the EFO corresponding to a reconstructed muon was included in a jet then the muon was considered to be associated with the jet.

The event inelasticity y was reconstructed from the Jacquet-Blondel estimator $y_{\text{JB}} = (E - p_Z)/(2E_e)$ [18], where $E - p_Z = \sum_i E^i - p_Z^i$ and the sum runs over all EFOs.

A sample of events with one muon and two jets was selected by requiring:

- ≥ 1 muon in one of the three muon-chamber regions defined in Eq. (1);
- ≥ 2 jets with pseudorapidity $|\eta^{\,\text{jet}}| < 2.5$, and transverse momentum $p_T^{\text{jet}} > 7\,\text{GeV}$ for the highest-p_T^{jet} jet and $p_T^{\text{jet}} > 6\,\text{GeV}$ for the second-highest-p_T^{jet} jet;
- that the muon was associated with any jet with $p_T^{\text{jet}} > 6\,\text{GeV}$ and $|\eta^{\,\text{jet}}| < 2.5$. To assure a reliable $p_{\text{T}}^{\text{rel}}$ measurement (see Section 5), the residual jet transverse momentum, calculated excluding the associated muon, was required to be greater than 2 GeV;
- a reconstructed vertex compatible with the nominal interaction point;
- no scattered-electron candidate found in the CAL;
- $0.2 < y_{\text{JB}} < 0.8$.

The last two cuts suppress background from high-Q^2 events and from non-ep interactions, and correspond to an effective cut $Q^2 < 1\,\text{GeV}^2$ and $0.2 < y < 0.8$.

After this selection, a sample of 3660 events remained.

4 Acceptance corrections and background simulation

To evaluate the detector acceptance and to provide the signal and background distributions, Monte Carlo (MC) samples of beauty, charm and light-flavour (LF) events were generated, corresponding respectively to six, five and three times the luminosity of the data. PYTHIA 6.2 [19, 20] was used as the reference MC, and HERWIG 6.1 [21] for systematic checks. The branching ratios for direct semi-leptonic $b \to \mu X$ decays and for indirect cascade decays into muons via charm, anti-charm, $\tau^{\pm}$ and J/ψ, were set to $\mathcal{B}_{\rm dir} = 0.106 \pm 0.002$ and $\mathcal{B}_{\rm indir} = 0.103 \pm 0.007$ [22], respectively. The distribution of the decay-lepton momentum in the B-meson centre-of-mass system from PYTHIA and HERWIG has been compared with measurements from e^+e^- collisions [23] and found to be in good agreement. The generated events were passed through a full simulation of the ZEUS detector based on GEANT 3.13 [24]. They were then subjected to the same trigger requirements and processed by the same reconstruction programs as for the data.

Figure 1 shows the kinematic distributions of $p_T^{\rm jet}$ and $\eta^{\rm jet}$ for the jet associated with the muon, as well as for highest-p_T jet that was not associated with a muon (other jet). The muon kinematic variables p_T^{μ} and η^{μ} are displayed, as well as $x_\gamma^{\rm jets}$, the fraction of the total hadronic $E - p_Z$ carried by the two highest-p_T jets[3]

$$x_\gamma^{\rm jets} = \frac{\sum_{j=1,2}(E^{\rm jet} - p_Z^{\rm jet})}{E - p_Z}. \qquad (2)$$

The data are compared in shape to the PYTHIA MC sample in which the relative fractions of beauty, charm and LF were mixed according to the cross sections predicted by the simulation. The comparison shows that the main features of the dijet-plus-muon sample are well reproduced by this MC mixture. The PYTHIA MC predicts that the non-$b\bar{b}$ background comprises 57% prompt muons from charmed-hadron decays and 43% muons from light-flavour hadrons, mostly due to in-flight decays of π and K mesons, with a small amount ($\sim 5\%$ of the LF component) from muons produced in interactions with the detector material. The punch-through contribution is negligible. The HERWIG Monte Carlo (not shown) also gives a good description of the data.

The detector acceptance for the final cross sections was calculated using the $b\bar{b}$ PYTHIA Monte Carlo, in which events were reweighted such that the transverse momentum distribution of the b quark agreed with that of the NLO calculations. The effects of this reweighting on the distributions in Fig.1 was small.

[3] $x_\gamma^{\rm jets}$ is the massive-jets analogue of the $x_\gamma^{\rm obs}$ variable used for massless jets in other ZEUS publications [25].

5 Signal extraction and cross section measurement

Because of the large b-quark mass, muons from semi-leptonic B-hadron decays tend to be produced with large transverse momentum with respect to the direction of the jet containing the B-hadron. The beauty signal was extracted by exploiting the distribution of the transverse momentum of the muon with respect to the momentum of the rest of the associated jet, $p_{\mathrm{T}}^{\mathrm{rel}}$, defined as:

$$p_{\mathrm{T}}^{\mathrm{rel}} = \frac{|\boldsymbol{p}^{\,\mu} \times (\boldsymbol{p}^{\,\mathrm{jet}} - \boldsymbol{p}^{\,\mu})|}{|\boldsymbol{p}^{\,\mathrm{jet}} - \boldsymbol{p}^{\,\mu}|}, \tag{3}$$

where $\boldsymbol{p}^{\,\mu}$ is the muon and $\boldsymbol{p}^{\,\mathrm{jet}}$ the jet momentum vector. Figure 2a shows the distributions, normalized to unity, of the reconstructed muon $p_{\mathrm{T}}^{\mathrm{rel}}$ as obtained from the Pythia MC, for beauty ($f_\mu^{b\bar{b},\mathrm{MC}}$), charm ($f_\mu^{c\bar{c},\mathrm{MC}}$) and LF ($f_\mu^{\mathrm{LF,MC}}$) events. The $p_{\mathrm{T}}^{\mathrm{rel}}$ distribution for beauty peaks at ~ 2 GeV and is well separated from those from charm and LF which are peaked close to zero. Since the shapes of $f_\mu^{\mathrm{LF,MC}}$ and $f_\mu^{c\bar{c},\mathrm{MC}}$ are very similar, the fraction of beauty ($a_{b\bar{b}}$) and background (a_{bkg}) events in the sample was obtained from a two-component fit to the shape of the measured $p_{\mathrm{T}}^{\mathrm{rel}}$ distribution f_μ with a beauty and a background component:

$$f_\mu = a_{\mathrm{bkg}} f_\mu^{\mathrm{bkg}} + a_{b\bar{b}} f_\mu^{b\bar{b}}, \tag{4}$$

where the $p_{\mathrm{T}}^{\mathrm{rel}}$ distribution of beauty, $f_\mu^{b\bar{b}}$, was taken from the Pythia MC: $f_\mu^{b\bar{b}} = f_\mu^{b\bar{b},\mathrm{MC}}$, and that of the background, f_μ^{bkg}, was obtained as explained below.

The distribution f_μ^{bkg} was obtained from the sum of a LF, f_μ^{LF}, and a charm, $f_\mu^{c\bar{c}}$, distribution weighted according to the charm fraction r obtained from the charm and LF cross sections given by Pythia:

$$f_\mu^{\mathrm{bkg}} = r f_\mu^{c\bar{c}} + (1-r) f_\mu^{\mathrm{LF}}. \tag{5}$$

The distribution f_μ^{LF} can be obtained from the $p_{\mathrm{T}}^{\mathrm{rel}}$ distribution of a sample of CTD tracks not identified as muons but fulfilling the same momentum and angular requirements applied to muons (called "unidentified tracks" in the following). The $p_{\mathrm{T}}^{\mathrm{rel}}$ distribution for unidentified tracks, f_x, is expected to be similar to f_μ^{LF}, under the assumption that the probability for an unidentified track (typically a π or a K meson) to be identified as a muon, $P_{x\to\mu}$, does not depend strongly on $p_{\mathrm{T}}^{\mathrm{rel}}$. This assumption is validated by the MC, since the MC distributions for the LF background, $f_\mu^{\mathrm{LF,MC}}$, and for the unidentified tracks, f_x^{MC}, are indeed very similar, as shown in Fig. 2a.

Figure 2b shows the f_x distribution obtained from a dijet sample selected without muon requirements. The shape obtained from Pythia, f_x^{MC}, underestimates the tail (for example by 24% at 2.625 GeV). The $p_{\mathrm{T}}^{\mathrm{rel}}$ shape of the LF background was therefore obtained

as

$$f_\mu^{\rm LF} = f_x \frac{f_\mu^{\rm LF,MC}}{f_x^{\rm MC}}, \tag{6}$$

where the ratio $f_\mu^{\rm LF,MC}/f_x^{\rm MC}$ is a MC-based correction that accounts for possible differences between $f_\mu^{\rm LF}$ and f_x due to a residual $p_{\rm T}^{\rm rel}$ dependence of $P_{x\to\mu}$ and to the charm and beauty contamination ($\sim 28\%$ and $\sim 2\%$ of respectively) in the dijet sample.

The data cannot be used to extract the distribution $f_\mu^{c\bar{c}}$. Two cases were therefore considered: the distribution given by the PYTHIA MC, $f_\mu^{c\bar{c},{\rm MC}}$, and the distribution obtained from the unidentified track sample, as in the case of the LF background: $f_x \frac{f_\mu^{c\bar{c},{\rm MC}}}{f_x^{\rm MC}}$. The average of these two cases was then taken as the nominal $f_\mu^{c\bar{c}}$:

Figure 3 shows the result of the $p_{\rm T}^{\rm rel}$ fit for muons in the rear, barrel and forward regions. The sum of the two components reproduces the data reasonably well. The fraction of b in the total sample of dijet events with a muon is $a_{b\bar{b}} = 0.224 \pm 0.017$ (stat.). In the determination of the cross sections, the fraction of beauty events in the data was extracted by a fit performed in each cross-section bin.

All the cross sections reported in Section 8, with the exception of that for b quarks, are inclusive muon (or b-jet) cross sections, obtained by counting muons (or b-jets) rather than events. Muons coming from both direct and indirect b decays are considered to be part of the signal. The cross sections are given for dijet events passing the following requirements: $Q^2 < 1\,{\rm GeV}^2$, $0.2 < y < 0.8$ and at least two hadron-level jets with $p_T^{\rm jet_1} > 7\,{\rm GeV}$, $p_T^{\rm jet_2} > 6\,{\rm GeV}$ and $\eta^{\rm jet_1}, \eta^{\rm jet_2} < 2.5$. These jets were defined using the k_T algorithm on stable hadrons, where the weakly decaying B hadrons were considered stable. For dijet events with a muon passing the cuts of Eq. (1), the acceptance varies from 10% at low p_T^μ to 20% at large p_T^μ.

The cross sections were measured from data collected at two different centre-of-mass energies, $\sqrt{s} = 300\,{\rm GeV}$ and $\sqrt{s} = 318\,{\rm GeV}$. They were corrected to $\sqrt{s} = 318\,{\rm GeV}$ using the NLO QCD prediction. The effect of this correction on the final cross section is $\sim 2\%$.

6 Theoretical predictions and uncertainties

The measured cross sections are compared to NLO QCD predictions based on the FMNR [26] program. The parton distribution functions used for the nominal prediction were GRVG-HO [27] for the photon and CTEQ5M [28] for the proton. The b-quark mass was set to $m_b = 4.75$ GeV, and the renormalisation and factorisation scales to the transverse mass, $\mu_r = \mu_f = m_T = \sqrt{\frac{1}{2}\left((p_T^b)^2 + (p_T^{\bar{b}})^2\right) + m_b^2}$, where $p_T^{b(\bar{b})}$ is the transverse momentum of the b ($\bar{b}$) quark in the laboratory frame. Jets were reconstructed by running the k_T

algorithm on the four momenta of the b and $\bar{b}$ quarks and of the third light parton (if present) generated by the program. The fragmentation of the b quark into a B hadron was simulated by rescaling the quark three-momentum (in the frame in which $p_Z^b = -p_Z^{\bar{b}}$, obtained with a boost along Z) according to the Peterson [29] fragmentation function with $\epsilon = 0.0035$. The muon momentum was generated isotropically in the B-hadron rest frame from the decay spectrum given by PYTHIA, which is in good agreement with measurements made at B factories [23].

To evaluate the uncertainty on the NLO calculations, the b-quark mass and the renormalisation and factorisation scales were varied simultaneously, to maximize the change, from $m_b = 4.5$ GeV and $\mu_r = \mu_f = m_T/2$ to $m_b = 5.0$ GeV and $\mu_r = \mu_f = 2m_T$, producing a variation in the cross section from $+34\%$ to -22%. The effect on the cross section of a variation of the Peterson parameter ϵ from 0.002 to 0.0055 [30] and of a change of the fragmentation function from the Peterson to the Kartvelishvili parametrisation (with $\alpha = 13$, as obtained from comparisons between NLO QCD and MC distributions) [31,32] was less than $\pm 3\%$. The effects of using different sets of parton densities and of a variation of the strong coupling constant ($\Lambda^{(5)}_{\rm QCD} = 0.226 \pm 0.025$ MeV) were all within $\pm 4\%$.

The NLO cross sections, calculated for jets made of partons, were corrected for jet hadronization effects to allow a direct comparison with the measured hadron-level cross sections. The corrections were derived from the MC simulation as the ratio of the hadron-level to the parton-level MC cross section, where the parton level is defined as being the result of the parton showering stage of the simulation. The average between the corrections obtained from PYTHIA and HERWIG was taken as the central value and their difference as the uncertainty. The effect of the hadronization correction was largest in the rear region, where the cross section was reduced by $(20 \pm 6)\%$ and smallest at large p_T^μ where it was reduced by $(3.0 \pm 0.3)\%$.

The measured cross sections are also compared to the absolute predictions of two MC models, PYTHIA 6.2 and CASCADE 1.1. The predictions of PYTHIA 6.2 were obtained [20] by mixing direct- ($\gamma g \to b\bar{b}$) and resolved-photon ($gg \to b\bar{b}$, $q\bar{q} \to b\bar{b}$) flavour-creation processes calculated using massive matrix elements and the flavour-excitation (FE) processes ($bg \to bg$, $bq \to bq$), in which a heavy quark is extracted from the photon or proton parton density. The FE processes contribute about 27% of the total $b\bar{b}$ cross section. The small ($\sim 5\%$) contribution from gluon splitting in parton showers ($g \to b\bar{b}$) was not included. The parton density CTEQ4L [33] was used for the proton and GRVG-LO [27] for the photon; the b-quark mass was set to 4.75 GeV and the b-quark string fragmentation was performed according to the Peterson function with $\epsilon = 0.0041$ [34].

CASCADE [35] is a Monte Carlo implementation of the CCFM evolution equations [36]. Heavy-quark production is obtained from the $O(\alpha_s)$ matrix elements for the process $\gamma g^* \to b\bar{b}$, in which the initial gluon can be off-shell. The gluon density, unintegrated in transverse

momentum (k_T), is obtained from an analysis of the proton structure functions based on the CCFM equations [37]; in the event generation the gluon density used corresponds to the set named "J2003 set 2". The mass of the b quark was set to 4.75 GeV and α_s was evaluated at the scale m_T. As for PYTHIA, the b-quark string fragmentation was performed according to the Peterson function with $\epsilon = 0.0041$.

7 Systematic uncertainties

The main experimental uncertainties are described below:

- the muon acceptance, including the efficiency of the muon chambers, of the reconstruction and of the MUON-CTD matching, is known to about 10% from a study based on an independent dimuon sample [38];
- the uncertainty on the $p_{\mathrm{T}}^{\mathrm{rel}}$ shape of the LF and charm background was evaluated by:
  - varying the charm fraction in the background, r, by $\pm 20\%$. This range was obtained by fixing the absolute charm-MC normalisation to a measurement of the charm dijet cross section [39] and using the PYTHIA or HERWIG MC to extrapolate to the kinematic range of the present measurement;
  - varying the jet-track association in the unidentified-track sample;
  - extracting f_{μ}^{LF} from a sample of unidentified CTD tracks, reweighted with a MC-based parametrisation of $P_{x\to\mu}$ depending on polar angle and momentum;
  - varying the $p_{\mathrm{T}}^{\mathrm{rel}}$ shape of the charm component of the background between the prediction from PYTHIA and the value obtained from the unidentified track sample;
  - using HERWIG instead of PYTHIA to simulate the background.

  The total uncertainty from these sources is about 10%. As a cross-check, a different definition of $p_{\mathrm{T}}^{\mathrm{rel}}$ was used to extract the beauty fraction, namely the transverse momentum of the muon with respect to the whole jet, including the muon itself, as used in a previous ZEUS publication [9]. The results were found to be in good agreement;
- the 2% uncertainty on the direct-decay branching ratio $\mathcal{B}_{\mathrm{dir}}$ introduces a 2% uncertainty on the b-jet and on the b-quark cross sections while it has no effect on the visible muon cross sections. The 7% uncertainty on the branching ratio for indirect decays $\mathcal{B}_{\mathrm{indir}}$ produces an uncertainty of 1% on the measured cross sections;
- the uncertainties on the dijet selection, on the energy scale, on the jet and y_{JB} resolution and trigger efficiency add up to a 7% uncertainty on the cross sections.

The uncertainty arising from the model dependence of the acceptance was evaluated as follows (the effect on the cross sections is shown in parenthesis):

- the Peterson fragmentation parameter ϵ in the MC was varied from 0.002 to 0.006 as allowed by LEP and SLD measurements [34, 40, 41]. The Lund-Bowler fragmentation function was used as an alternative, both with the default PYTHIA parameters and with parameters taken from OPAL measurements [34] ($\pm$2%);
- instead of using PYTHIA reweighted to the NLO p_T^b distribution it was reweighted as a function of $\eta^{\,\mathrm{jet}}$ and p_T^{jet} to agree with the measured differential distributions (-2%) or without reweighting (+2%);
- the fraction of flavour-excitation events in PYTHIA was varied up and down by a factor two ($\pm$ 4%), as allowed by comparisons to the x_γ^{jets} distribution of the data;
- HERWIG was used instead of PYTHIA (-2%).

The total systematic uncertainty was obtained by adding the above contributions in quadrature. A 2% overall normalization uncertainty associated with the luminosity measurement was not included.

8 Results

All the cross sections reported below, except for the b-quark cross section, are given for dijet events with $p_T^{\mathrm{jet}_1}, p_T^{\mathrm{jet}_2} > 7, 6\,\mathrm{GeV}$, $\eta^{\,\mathrm{jet}_1}, \eta^{\,\mathrm{jet}_2} < 2.5$, $Q^2 < 1\,\mathrm{GeV}^2$ and $0.2 < y < 0.8$.

The first set of measurements are beauty cross sections for muons passing the cuts defined in Eq. (1). The results for the forward, barrel and rear muon-chamber regions are shown in Fig. 4a and Table 1 and compared with the NLO prediction and MC models. Both the NLO and the MC models are in reasonable agreement with the data.

Figure 4b and Table 2 show the differential cross-section $d\sigma/dx_\gamma^{\mathrm{jets}}$ for muons in the range defined by Eq. (1) in dijet events. The x_γ^{jets} variable corresponds at leading order to the fraction of the exchanged-photon momentum in the hard scattering process. It provides a tool to measure the relative importance of photon-gluon fusion, $\gamma g \to b\bar{b}$, which gives a peak at $x_\gamma^{\mathrm{jets}} \sim 1$, and of other contributions, such as gluon-gluon fusion (with a gluon coming from the photon) or higher-order diagrams, which are distributed over the whole x_γ^{jets} range. The sample is dominated by the high-x_γ^{jets} peak but a low-x_γ^{jets} component is also apparent. The NLO QCD prediction describes the distribution well. PYTHIA is also able to give a good description of the data due to the large contribution from flavour excitation at low x_γ^{jets}. CASCADE, which generates low-x_γ^{jets} events via initial-state radiation without using a parton density in the photon, tends to underestimate the cross section at low x_γ^{jets}.

The differential cross sections in the muonic variables were measured for $p_T^\mu > 2.5\,\mathrm{GeV}$ and $-1.6 < \eta^\mu < 2.3$. Figure 5 and Table 3 show the differential cross-sections $d\sigma/d\eta^\mu$

and $d\sigma/dp_T^\mu$ for muons in dijet events. The NLO QCD predictions and the MC models describe the η^μ distribution well. The p_T^μ distribution is well reproduced by NLO QCD while the p_T^μ slope tends to be too soft in CASCADE and PYTHIA.

The jet associated with the muon (or μ-jet) reproduces the kinematics of the b (or $\bar{b}$) quark to a good approximation. The μ-jet is defined as the jet containing the B hadron that decays into the muon. Figure 6a-b and Table 4 show the differential cross section for the jet associated with a muon passing the cuts of Eq. (1) as a function of the jet pseudorapidity, $d\sigma/d\eta^{\mu\text{-jet}}$, and transverse momentum, $d\sigma/dp_T^{\mu\text{-jet}}$, for $\eta^{\mu\text{-jet}} < 2.5$ and $p_T^{\mu\text{-jet}} > 6\,\text{GeV}$. The μ-jet distributions are well reproduced by the NLO and by the MC models.

The μ-jet cross sections have been corrected to obtain the cross sections for b-jets in dijet events: $\sigma(ep \to e'\,jj\,X)$. A b-jet is defined as a jet containing a B (or an anti-B) hadron. This correction was performed using PYTHIA and accounts for the $b \to \mu$ branching ratio, including direct and indirect decays, and for the full muon phase space. Figure 6c-d and Table 5 show the differential cross-sections $d\sigma/d\eta^{b\text{-jet}}$ and $d\sigma/dp_T^{b\text{-jet}}$. The level of agreement of b jets with the NLO QCD and MC predictions is similar to that found for the μ jets. It should be noted that the hadronization corrections in the first two $\eta^{b\text{-jet}}$ bins are large ($\sim -20\%$).

To compare the present result with a previous ZEUS measurement given at the b-quark level, the NLO QCD prediction was used to extrapolate the cross section for dijet events with a muon to the inclusive b-quark cross section. The b-quark differential cross section as a function of the quark transverse momentum, $d\sigma(ep \to bX)/dp_T^b$, for b-quark pseudorapidity in the laboratory frame $|\eta^b| < 2$ (corresponding to a rapidity in the ep centre of mass of $-3.75 < Y^b_{\text{cms}} < 0.25$), for $Q^2 < 1\,\text{GeV}^2$ and $0.2 < y < 0.8$, was obtained from the dijet cross section for events with a μ-jet within $|\eta^{\mu\text{-jet}}| < 2$ using the NLO prediction corrected for hadronization. The $\bar{b}$ quark was not considered in the definition of the b-quark cross section. As a cross-check, the measurement was corrected to the b-quark level using the PYTHIA MC, giving a result in agreement within 6%. The result, shown in Figure 7 and Table 6, is compared to the previous ZEUS measurement [9] of the b-quark cross section for $p_T^b > p_T^{\min} = 5\,\text{GeV}$ and $|\eta^b| < 2$, translated into a differential cross section using the NLO prediction and plotted at the average b-quark transverse momentum, $\langle p_T^b \rangle$, of the accepted events taken from the Monte Carlo:

$$\left(\frac{d\sigma}{dp_T^b}\right)_{\langle p_T^b\rangle} = \left(\frac{d\sigma^{\text{NLO}}}{dp_T^b}\right)_{\langle p_T^b\rangle} \frac{\sigma(p_T^b > p_T^{\min})}{\sigma^{\text{NLO}}(p_T^b > p_T^{\min})}.$$

The two independent measurements are consistent and in agreement with the NLO QCD predictions.

9 Conclusions

Beauty production identified by semi-leptonic decay into muons has been measured in dijet events with $Q^2 < 1\,\mathrm{GeV}^2$. Differential cross sections for the reaction $ep \to e'\, b\bar{b}\, X \to e'\, jj\mu\, X'$ have been measured as a function of the pseudorapidity and transverse momentum of the muon and of x_γ^{jets}. Differential cross sections for the production of b-jets were also measured.

The results were compared to MC models and to a NLO QCD prediction combined with fragmentation and B-hadron decay models. This prediction is in good agreement with the data in all the differential distributions. The PYTHIA MC model is also able to give a reasonable description of the differential cross sections. The CASCADE MC model also gives a reasonable description of the data, except for the low-x_γ^{jets} region.

The large excess of the first measurement of beauty photoproduction over NLO QCD, reported by the H1 collaboration [8], is not confirmed. The present result is consistent with the previous ZEUS measurement using semi-leptonic B decays into electrons [9]. Beauty photoproduction in ep collisions is reasonably well described both by NLO QCD and by a MC model that includes a substantial flavour excitation component.

Acknowledgements

We thank the DESY Directorate for their strong support and encouragement. The remarkable achievements of the HERA machine group were essential for the successful completion of this work and are greatly appreciated. We are grateful for the support of the DESY computing and network services. The design, construction and installation of the ZEUS detector have been made possible owing to the ingenuity and effort of many people who are not listed as authors. It is also a pleasure to thank S. Frixione and H. Jung for help with theoretical predictions and useful conversation.

μ-chambers	Muons	$a_{b\bar{b}}$	$\sigma \pm$ stat. $\pm$ syst. (pb)	$\sigma^{NLO} \times C_{had}$ (pb)	C_{had}
rear	484	0.15	$6.5 \pm 1.5^{+1.0}_{-1.1}$	$4.3^{+1.6}_{-1.0}$	0.80
barrel	2316	0.25	$38.2 \pm 3.4^{+5.7}_{-5.8}$	$33.9^{+11.0}_{-7.0}$	0.89
forward	868	0.21	$16.6 \pm 3.3^{+2.9}_{-4.6}$	$6.5^{+2.8}_{-1.6}$	0.86

Table 1: *For each muon-chamber region defined in Eq. (1) the columns show: the number of selected muons; the beauty fraction $a_{b\bar{b}}$ obtained from the $p_{\mathrm{T}}^{\mathrm{rel}}$ fit; the measured beauty cross section with the statistical and systematic uncertainties; the NLO QCD prediction corrected to the hadron level with the theoretical uncertainty and the hadronization correction. For further details see the caption to Fig. 4.*

x_γ^{jets} range	$d\sigma/dx_\gamma^{\mathrm{jets}} \pm$ stat. $\pm$ syst. (pb)	C_{had}
0.00, 0.25	$12.9 \pm 6.7^{+4.2}_{-7.2}$	0.68
0.25, 0.50	$20.8 \pm 7.2^{+8.2}_{-7.7}$	0.83
0.50, 0.75	$30.0 \pm 5.2^{+6.4}_{-4.1}$	0.86
0.75, 1.00	$165 \pm 14^{+22}_{-34}$	0.90

Table 2: *Differential muon cross section as a function of x_γ^{jets}. The multiplicative hadronization correction applied to the NLO prediciton is shown in the last column. For further details see the caption to Fig. 4.*

η^μ range	$d\sigma/d\eta^\mu \pm$ stat. $\pm$ syst. (pb)	C_{had}
-1.6, -0.75	$4.6 \pm 1.3^{+0.8}_{-0.9}$	0.83
-0.75, 0.25	$18.8 \pm 2.2^{+2.7}_{-2.7}$	0.88
0.25, 1.30	$16.7 \pm 2.4^{+2.7}_{-2.9}$	0.92
1.30, 2.30	$10.0 \pm 2.3^{+1.4}_{-2.6}$	0.91
p_T^μ range (GeV)	$d\sigma/dp_T^\mu \pm$ stat. $\pm$ syst. (pb/GeV)	C_{had}
2.5, 4.0	$16.1 \pm 2.3^{+2.9}_{-3.7}$	0.87
4.0, 6.0	$7.1 \pm 1.0^{+1.3}_{-1.2}$	0.92
6.0, 10.0	$1.69 \pm 0.32^{+0.22}_{-0.24}$	0.97

Table 3: *Differential muon cross section as a function of η^μ and p_T^μ. For further details see the caption to Fig. 5.*

$\eta^{\mu\text{-jet}}$ range	$d\sigma/d\eta^{\mu\text{-jet}} \pm$ stat. $\pm$ syst. (pb)	C_{had}
-1.6,-0.6	$8.6 \pm 1.7^{+1.4}_{-1.8}$	0.73
-0.6, 0.4	$18.9 \pm 2.2^{+2.8}_{-2.7}$	0.84
0.4, 1.4	$14.3 \pm 2.3^{+2.5}_{-3.8}$	0.97
1.4, 2.5	$14.4 \pm 2.7^{+2.3}_{-4.2}$	1.00
$p_T^{\mu\text{-jet}}$ range (GeV)	$d\sigma/dp_T^{\mu\text{-jet}} \pm$ stat. $\pm$ syst. (pb/GeV)	C_{had}
6,11	$6.41 \pm 0.67^{+1.00}_{-1.24}$	0.88
11,16	$2.98 \pm 0.37^{+0.52}_{-0.82}$	0.88
16,30	$0.51 \pm 0.11^{+0.08}_{-0.08}$	0.90

Table 4: *Differential cross section for jets associated with a muon as a function of $\eta^{\mu\text{-jet}}$ and $p_T^{\mu\text{-jet}}$. For further details see the caption to Fig. 6.*

$\eta^{b\text{-jet}}$ range	$d\sigma/d\eta^{b\text{-jet}} \pm$ stat. $\pm$ syst. (pb)	C_{had}
-1.6,-0.6	$152 \pm 29^{+24}_{-31}$	0.68
-0.6, 0.4	$356 \pm 41^{+59}_{-53}$	0.78
0.4, 1.4	$275 \pm 45^{+53}_{-73}$	0.96
1.4, 2.5	$229 \pm 44^{+41}_{-69}$	1.06
$p_T^{b\text{-jet}}$ range (GeV)	$d\sigma/dp_T^{b\text{-jet}} \pm$ stat. $\pm$ syst. (pb/GeV)	C_{had}
6,11	$137 \pm 14^{+21}_{-27}$	0.85
11,16	$43.8 \pm 5.5^{+7.7}_{-12.0}$	0.86
16,30	$5.7 \pm 1.2^{+1.0}_{-0.9}$	0.89

Table 5: *Differential cross section for b-jets as a function of $\eta^{b\text{-jet}}$ and $p_T^{b\text{-jet}}$. For further details see the caption to Fig. 6.*

$p_T^{\mu\text{-jet}}$ range (GeV)	$d\sigma/dp_T^{\mu\text{-jet}} \pm \text{stat.} \pm \text{syst.}$ ($\lvert\eta^{\mu\text{-jet}}\rvert < 2$) (pb/GeV)	C_{had}	$\langle p_T^b \rangle$ (GeV)	$d\sigma/dp_T^b \pm \text{stat.} \pm \text{syst.}$ (pb/GeV)
6,11	$6.22 \pm 0.63^{+0.91}_{-1.04}$	0.87	8.5	$90 \pm 9^{+13}_{-15}$
11,16	$2.74 \pm 0.36^{+0.47}_{-0.74}$	0.88	13.6	$18.2 \pm 2.4^{+3.1}_{-4.9}$
16,30	$0.43 \pm 0.10^{+0.07}_{-0.06}$	0.88	21.25	$2.0 \pm 0.5^{+0.3}_{-0.3}$

Table 6: *Differential b-quark cross-section $d\sigma/dp_T^b$. The first columns show the differential μ-jet cross-section $d\sigma/dp_T^{\mu\text{-jet}}$ restricted to $|\eta^{\mu\text{-jet}}| < 2$, the corresponding hadronization correction and the average b-quark transverse momentum, $\langle p_T^b \rangle$, as obtained from the* PYTHIA *MC. The b-quark differential cross section $d\sigma/dp_T^b$ for $|\eta^b| < 2$, evaluated at $\langle p_T^b \rangle$, is shown in the last column. For further details see the caption to Fig. 7.*

References

[1] S. Frixione et al., Nucl. Phys. **B 454**, 3 (1995);
M. Cacciari, S. Frixione and P. Nason, JHEP **0103**, 006 (2001).

[2] M. Basile et al., Lett. Nuovo Cim. **31**, 97 (1981).

[3] UA1 Coll., C. Albajar et al., Phys. Lett. **B 256**, 121 (1991). Erratum-ibid. **B 262**, 497 (1991);
UA1 Coll., C. Albajar et al., Z. Phys. **C 61**, 41 (1994).

[4] CDF Coll., F. Abe et al., Phys. Rev. Lett. **71**, 500 (1993);
CDF Coll., F. Abe et al., Phys. Rev. Lett. **71**, 2396 (1993);
CDF Coll., F. Abe et al., Phys. Rev. Lett. **75**, 1451 (1995);
CDF Coll., F. Abe et al., Phys. Rev. **D 53**, 1051 (1996);
CDF Coll., P. Acosta et al., Phys. Rev. **D 65**, 052005 (2002);
DØ Coll., S. Abachi et al., Phys. Rev. Lett. **74**, 3548 (1995);
DØ Coll., B. Abbott et al., Phys. Lett. **B 487**, 264 (2000);
DØ Coll., B. Abbott et al., Phys. Rev. Lett. **84**, 5478 (2000);
DØ Coll., B. Abbott et al., Phys. Lett. **85**, 5068 (2000).

[5] L3 Coll., M. Acciarri et al., Phys. Lett. **B 503**, 10 (2001).

[6] WA78 Coll., M. Catanesi et al., Phys. Lett. **B 202**, 453 (1988);
E672/E706 Coll., R. Jesik et al., Phys. Rev. Lett. **74**, 495 (1995).

[7] E771 Coll., T. Alexopoulos et al., Phys. Rev. Lett. **82**, 41 (1999);
D.M. Jansen et al., Phys. Rev. Lett. **74**, 3118 (1995);
HERA–B Coll., I. Abt et al., Eur. Phys. J. **C 26**, 345 (2003).

[8] H1 Coll., C.Adloff et al., Phys. Lett. **B 467**, 156 (1999). Erratum-ibid. **B 518**, 331 (2001).

[9] ZEUS Coll., J. Breitweg et al., Eur. Phys. J. **C 18**, 625 (2001).

[10] ZEUS Coll., U. Holm (ed.), *The ZEUS Detector*. Status Report (unpublished), DESY (1993), available on `http://www-zeus.desy.de/bluebook/bluebook.html`.

[11] N. Harnew et al., Nucl. Inst. Meth. **A 279**, 290 (1989);
B. Foster et al., Nucl. Phys. Proc. Suppl. **B 32**, 181 (1993);
B. Foster et al., Nucl. Inst. Meth. **A 338**, 254 (1994).

[12] M. Derrick et al., Nucl. Inst. Meth. **A 309**, 77 (1991);
A. Andresen et al., Nucl. Inst. Meth. **A 309**, 101 (1991);
A. Caldwell et al., Nucl. Inst. Meth. **A 321**, 356 (1992);
A. Bernstein et al., Nucl. Inst. Meth. **A 336**, 23 (1993).

[13] G. Abbiendi et al., Nucl. Instr. and Meth. **A 333**, 342 (1993).

[14] J. Andruszków et al., Preprint DESY-92-066, DESY, 1992;
ZEUS Coll., M. Derrick et al., Z. Phys. **C 63**, 391 (1994);
J. Andruszków et al., Acta Phys. Pol. **B 32**, 2025 (2001).

[15] ZEUS Coll., J. Breitweg et al., Eur. Phys. J. **C 1**, 81 (1998);
G.M. Briskin. Ph.D. Thesis, Tel Aviv University, (1998). DESY-THESIS-1999-036.

[16] S. Catani, Yu.L. Dokshitzer and B.R. Webber, Phys. Lett. **B 285**, 291 (1992).

[17] S.D. Ellis and D.E. Soper, Phys. Rev. **D 48**, 3160 (1993).

[18] F. Jacquet and A. Blondel, *Proceedings of the Study for an ep Facility for Europe*, U. Amaldi (ed.), p. 391. Hamburg, Germany (1979). Also in preprint DESY 79/48.

[19] T. Sjöstrand et al., Comp. Phys. Comm. **138**, 238 (2001).

[20] E. Norrbin and T. Sjöstrand, Eur. Phys. J. **C 17**, 137 (2000).

[21] G. Marchesini et al., Comp. Phys. Comm. **67**, 465 (1992).

[22] Particle Data Group, K. Hagiwara et al., Phys. Rev. **D 66**, 010001 (2002).

[23] Belle Coll., K. Abe et al., Phys. Lett. **B 547**, 181 (2002);
Babar Coll., B. Aubert et al., Phys. Rev. **D 67**, 031101 (2003).

[24] R. Brun et al., GEANT3, Technical Report CERN-DD/EE/84-1, CERN, 1987.

[25] ZEUS Coll., M. Derrick et al., Phys. Lett. **B 348**, 665 (1995).

[26] S. Frixione et al., Nucl. Phys. **B412**, 225 (1994).

[27] M. Gluck, E. Reya and A. Vogt, Phys. Rev. **D 46**, 1973 (1992).

[28] CTEQ Coll., H.L. Lai et al., Eur. Phys. J. **C 12**, 375 (2000).

[29] C. Peterson et al., Phys. Rev. **D 27**, 105 (1983).

[30] P. Nason and C. Oleari, Nucl. Phys. **B 565**, 245 (2000).

[31] V.G Kartvelishvili, A.K. Likhoded and V.A. Petrov, Phys. Lett. **B 78**, 615 (1978).

[32] M. Cacciari and P. Nason, Phys. Rev. Lett. **89**, 122003 (2002).

[33] H.L. Lai et al., Phys. Rev. **D 55**, 1280 (1997).

[34] OPAL Coll., G. Abbiendi et al., Eur. Phys. J. **C 29**, 463 (2003).

[35] H. Jung and G.P. Salam, Eur. Phys. J. **C 19** (2001);
H. Jung, Comp. Phys. Comm. **143**, 100 (2002).

[36] M. Ciafaloni, Nucl. Phys. **B 296**, 49 (1998);
S. Catani, F. Fiorani and G. Marchesini, Phys. Lett. **B 234**, 339 (1990).

[37] M. Hansson and H. Jung, Preprint hep/ph0309009, 2003.

[38] M. Turcato. Ph.D. Thesis, Padova University, (2002). DESY-THESIS-2003-039.

[39] ZEUS Coll., S. Chekanov et al., Phys. Lett. **B 565**, 87 (2003).

[40] ALEPH Coll., A. Heister et al., Phys. Lett. **B 512**, 30 (2001).

[41] SLD Coll., K. Abe et al., Phys. Rev. **D 65**, 092006 (2002). Erratum-ibid. **D 66**, 079905 (2002).

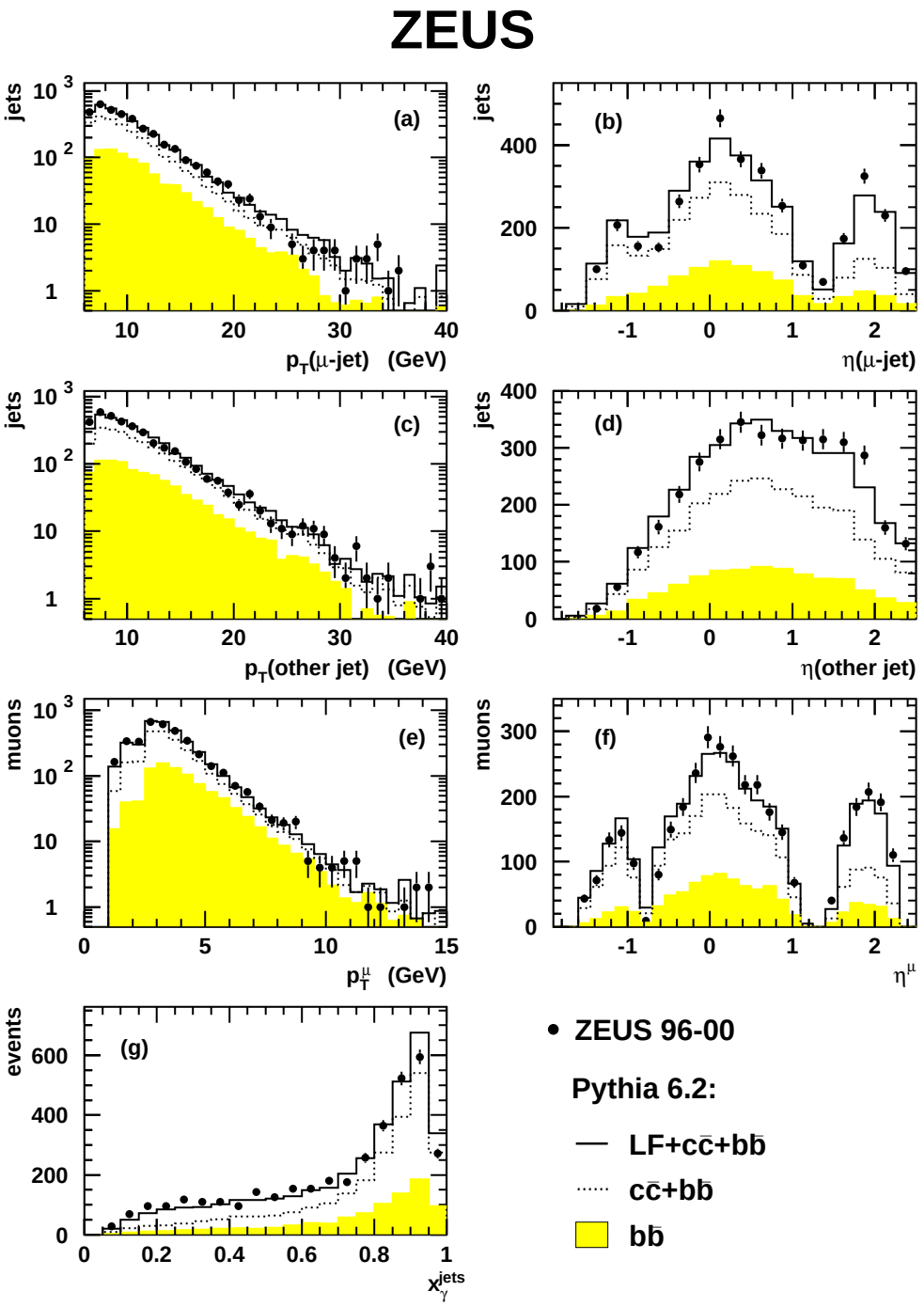

Figure 1: *Distributions for the dijet-plus-muon sample (points) compared to the predictions of the* PYTHIA *Monte Carlo (full line) normalized to the data. The shaded histogram shows the beauty component and the dotted line is the sum of charm and beauty. The plots show (a) the transverse momentum of the jet associated with the muon; (b) its pseudorapidity; (c) the transverse momentum of the highest-p_T non-μ-associated jet; (d) its pseudorapidity; (e) the transverse momentum of the muon; (f) its pseudorapidity; (g) the distribution of $x_\gamma^{\rm jets}$.*

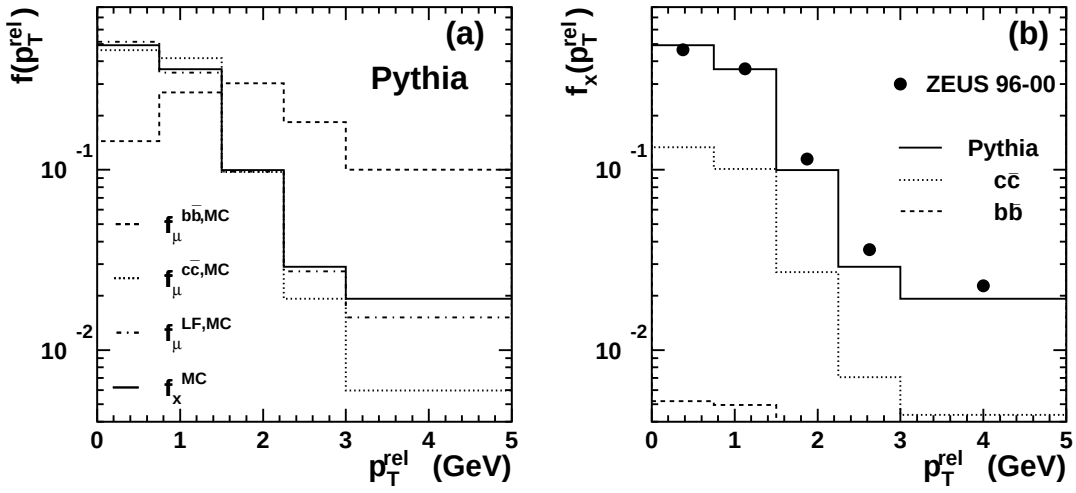

Figure 2: *(a) The $p_{\mathrm{T}}^{\mathrm{rel}}$ distribution as predicted by the* PYTHIA *Monte Carlo for reconstructed muons from beauty ($f_\mu^{b\bar{b},\mathrm{MC}}$, dashed histogram), charm ($f_\mu^{c\bar{c},\mathrm{MC}}$, dotted histogram) and light-flavours ($f_\mu^{\mathrm{LF},\mathrm{MC}}$, dash-dotted histogram), and for unidentified tracks (f_x^{MC}, full-line histogram). The distributions are normalized to unity. (b) The $p_{\mathrm{T}}^{\mathrm{rel}}$ distribution of unidentified data tracks (points), compared to the prediction from* PYTHIA *(full line). The charm and beauty components are also shown as the dotted- and dashed-line histograms, respectively.*

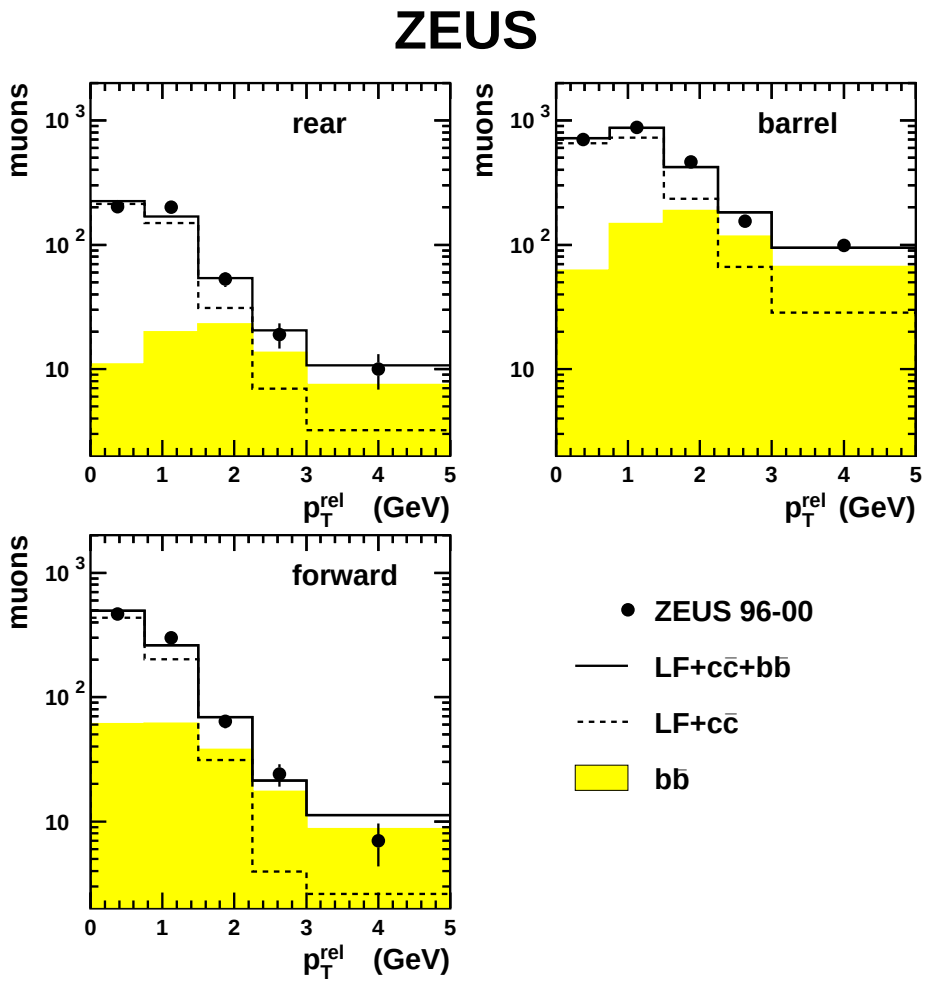

Figure 3: *The p_T^{rel} distribution for events with muons in the rear, barrel and forward regions defined in Eq. (1). The data (points) are compared to the mixture of beauty and charm+LF background obtained from the p_T^{rel} fit (full line). The shaded histogram represents the beauty component while the dashed-line histogram is the background.*

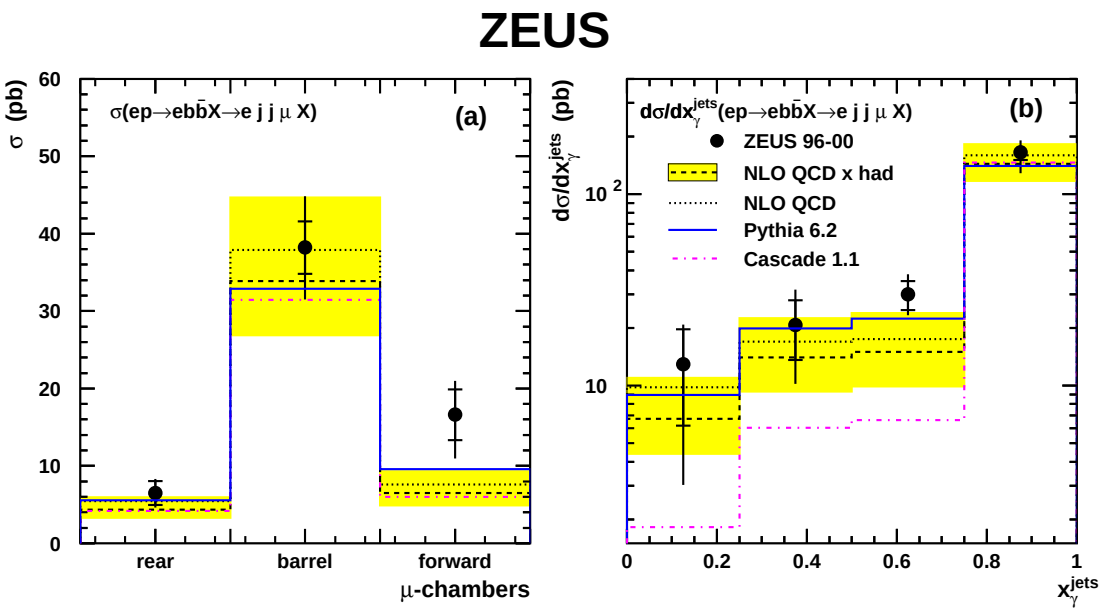

Figure 4: *Cross sections for muons coming from b decays in dijet events with* $p_T^{\mathrm{jet}_1} > 7, p_T^{\mathrm{jet}_2} > 6\ GeV$, $\eta^{\mathrm{jet}_1}, \eta^{\mathrm{jet}_2} < 2.5$, $0.2 < y < 0.8$, $Q^2 < 1\ GeV^2$ *passing the selection of Eq. (1). (a) The cross section for the forward, barrel and rear regions (defined in Eq. (1)). (b) The differential cross section as a function of* x_γ^{jets}. *The data (points) are compared to the predictions of NLO QCD (dotted line: parton-level jets; dashed line: jets corrected to the hadron level). The full error bars are the quadratic sum of the statistical (inner part) and systematic uncertainties. The band around the NLO prediction represents the variation on the theoretical predictions obtained by varying the b-quark mass,* μ_r *and* μ_f, *as explained in the text. The data are also compared to the predictions of the* PYTHIA *(solid line histogram) and* CASCADE *(dot-dashed line histogram) Monte Carlo models.*

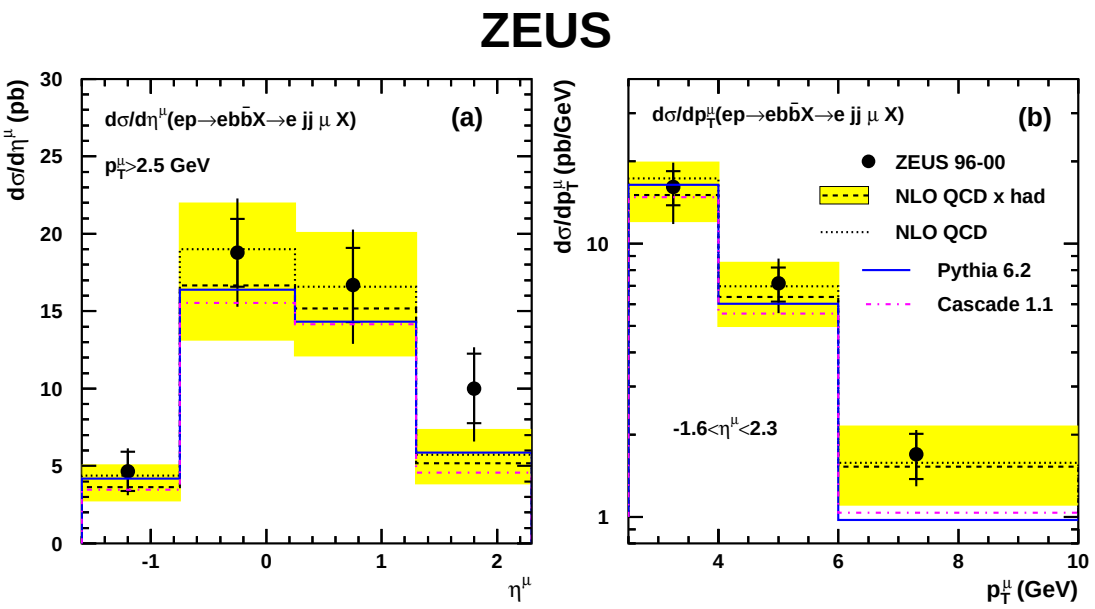

Figure 5: *Differential cross sections as a function of (a) the muon pseudorapidity η^μ and (b) transverse momentum p_T^μ, for $p_T^\mu > 2.5\,GeV$ and $-1.6 < \eta^\mu < 2.3$, for muons coming from b decays in dijet events with $p_T^{\mathrm{jet}_1} > 7, p_T^{\mathrm{jet}_2} > 6\,GeV$, $\eta^{\mathrm{jet}_1}, \eta^{\mathrm{jet}_2} < 2.5$, $0.2 < y < 0.8$, $Q^2 < 1\,GeV^2$. The data (points) are compared to the predictions of NLO QCD (dotted line: parton-level jets; dashed line: corrected to hadron-level jets). The full error bars are the quadratic sum of the statistical (inner part) and systematic uncertainties. The band around the NLO prediction represents the variation on the theoretical predictions obtained by varying the b-quark mass and μ_r and μ_f as explained in the text.The data are also compared to the predictions of the* PYTHIA *(solid line histogram) and* CASCADE *(dot-dashed line histogram) Monte Carlo models.*

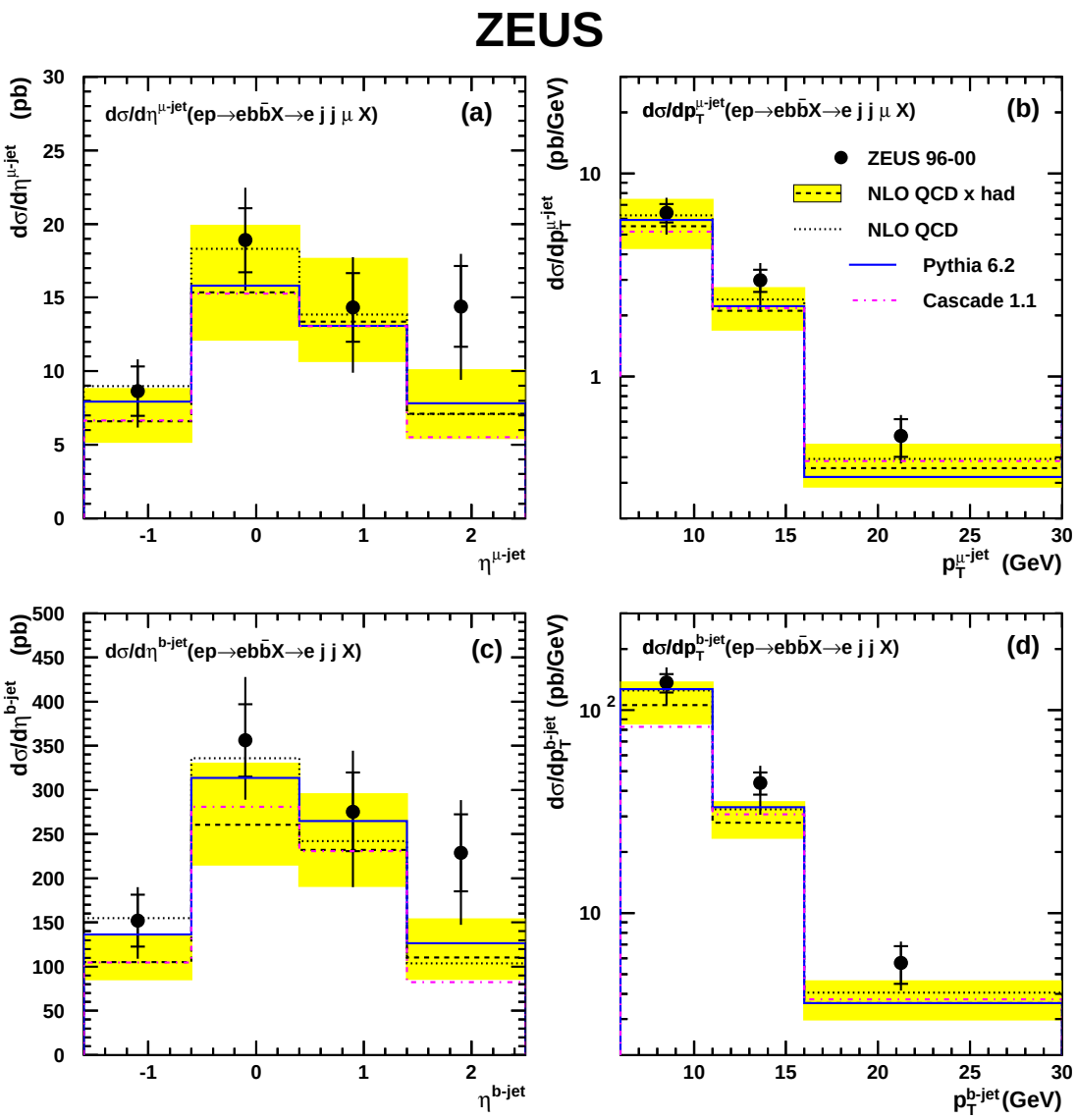

Figure 6: *Differential cross sections as a function of (a) the pseudorapidity $\eta^{\mu-\mathrm{jet}}$ and (b) the transverse momentum $p_T^{\mu-\mathrm{jet}}$ of the jet associated to the muon, for $p_T^{\mu-\mathrm{jet}} > 6\,GeV$, $\eta^{\mu-\mathrm{jet}} < 2.5$, for muons passing the selection of Eq. (1) and coming from b decays; differential cross sections as a function of (c) the pseudorapidity $\eta^{b-\mathrm{jet}}$ and (d) the transverse momentum $p_T^{b-\mathrm{jet}}$ of the jet containing a B hadron. All the cross sections are evaluated for dijet events with $p_T^{\mathrm{jet}_1} > 7, p_T^{\mathrm{jet}_2} > 6\,GeV$, $\eta^{\mathrm{jet}_1}, \eta^{\mathrm{jet}_2} < 2.5$, $0.2 < y < 0.8$, $Q^2 < 1\,GeV^2$. The data (points) are compared to the predictions of NLO QCD (dotted line: parton level; dashed line: corrected to hadron level). The full error bars are the quadratic sum of the statistical (inner part) and systematic uncertainties. The band around the NLO prediction represents the uncertainty on the theoretical prediction corrected for hadronization. The data are also compared to the predictions of the* PYTHIA *(solid line histogram) and* CASCADE *(dot-dashed line histogram) Monte Carlo models.*

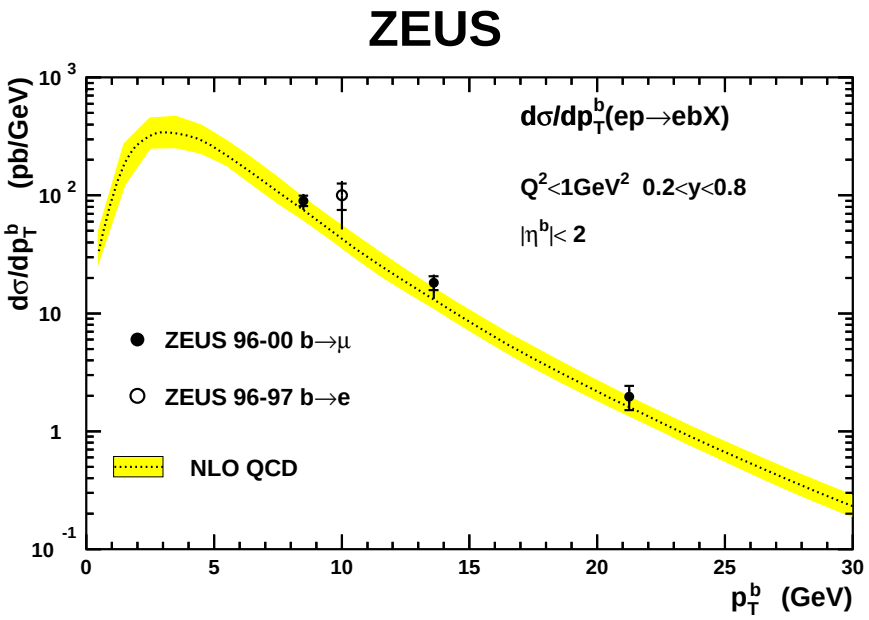

Figure 7: *Differential cross section for b-quark production as a function of the b-quark transverse momentum p_T^b for b-quark pseudorapidity $|\eta^b| < 2$ and for $Q^2 < 1\ GeV^2$, $0.2 < y < 0.8$. The filled points show the ZEUS results from this analysis and the open point is the previous ZEUS measurement in the electron channel [9]. The full error bars are the quadratic sum of the statistical (inner part) and systematic uncertainties. The dashed line shows the NLO QCD prediction with the theoretical uncertainty shown as the shaded band.*